

# Application of Spalart-Allmaras steady RANS-actuator disk model for horizontal-axis wind turbine simulation

VC Tai<sup>1\*</sup>, YC Tan<sup>1</sup>, LK Moey<sup>1</sup>, NFA Rahman<sup>2</sup> and D Baglee<sup>3</sup>

<sup>1</sup> Centre for Sustainable Design, Modelling and Simulation, SEGi University, 47810 PJ, Selangor, Malaysia

<sup>2</sup> Faculty of Engineering and Green Technology, Universiti Tunku Abdul Rahman, 31900 Kampar, Perak, Malaysia

<sup>3</sup> School of Engineering, Faculty of Technology, University of Sunderland, SR1 3SD, Sunderland, UK

\*E-mail: taivincent@segi.edu.my

**Abstract.** Accurate prediction of wind turbine (WT) wake is essential for optimising wind farm layouts and maximising energy production. Traditional wake models, such as the Jensen and Park models, are commonly used in WT simulations but often struggle to capture wake characteristics accurately. Furthermore, high-fidelity Computational Fluid Dynamics simulations are computationally intensive, limiting their applicability for large-scale simulations. This research introduces an innovative approach to WT wake modelling using the Spalart-Allmaras (SA) turbulence model within a steady Reynolds-Averaged Navier-Stokes framework, specifically applied to horizontal-axis WT. The turbulent length scale, which is essential for wake predictions in SA turbulence model, has been derived from the standard  $k-\epsilon$  turbulence model based on the neutral atmospheric boundary layer assumption. WT is modelled as actuator disk (AD), with thrust as a momentum source term distributed across the AD using a radial distribution function. Wake velocities are measured from 2.5 to 10 times the WT diameter downstream. The model's accuracy is validated using four WTs of varying sizes and operational conditions. The average mean absolute percentage error (MAPE) of 5.5% confirming that the SA model effectively captures wake profiles at multiple downstream locations. Additionally, the SA model achieves these results with significantly reduced computational costs compared to traditional two-equation turbulence models. These findings offer valuable insights for optimising turbine placement and improving wind farm performance, positioning this research as highly relevant for both academic and industrial applications.

**Keywords:** Actuator disk, Wake modelling, Spalart-Allmaras model, Turbulent length scale, Wind turbine



## 1. Introduction

The extraction of wind energy by wind turbines (WT) generates a wake [1], characterized by reduced wind speeds and increased turbulence, which can lead to significant power production losses within a wind farm. Therefore, accurate modelling and evaluation of wake losses are essential for optimizing wind farm layout, estimating energy production [2], and developing effective farm-level control strategies [3].

Actuator disk (AD) model is widely used in wake studies [3–5]. The two-equation Reynolds Averaged Navier-Stokes (RANS) turbulence models such as  $k - \omega$  [4] and  $k - \varepsilon$  [5–7] models are often employed to model the turbulent flow fields, where  $k$  is the turbulent kinetic energy,  $\varepsilon$  is the turbulent dissipation rate, and  $\omega$  is the specific turbulent dissipation rate. These two-equation models often require careful modelling of  $k$ ,  $\varepsilon$ , and  $\omega$  to mimic the effects induced by the WT. In a more advanced computational fluid dynamics (CFD) model, large eddy simulation (LES) is employed to consider the large scales eddies [8–10]. Though LES can generate relatively accurate results, the computational cost is much higher compared to the RANS models.

Spalart-Allmaras (SA) turbulence model is a family of RANS model [11]. Unlike two-equation models, the SA model solves a single transport equation for the SA variable, eliminating the need to model the variables  $k$  and  $\varepsilon$  or  $\omega$ . To the best of the authors' knowledge, no existing literature explores the use of the SA model in conjunction with the AD model for wake modelling. This paper aims to address this gap by proposing a method to determine the turbulent length scale ( $\ell_T$ ) for applying the SA model in horizontal-axis WT wake simulations using the AD approach.

## 2. Actuator disk model

WT is modelled as a disk in the model with a momentum source term,  $S_u$  [5]:

$$S_u = -\frac{1}{2}\rho\left(\frac{c_x}{\Delta x}\right)u_D^2 \quad (1)$$

Where  $\Delta x = 0.05D$  is the disk thickness,  $D$  is the rotor diameter,  $\rho$  is the air density,  $u_D = (1 - a)U_0$  is the disk velocity,  $c_x = C_T(1 - a)^{-2}$  is drag coefficient,  $a = (1 - \sqrt{1 - C_T})/2$  is the axial induction factor,  $U_0$  is freestream velocity, and  $C_T$  is the WT thrust coefficient.

## 3. Governing equations

### 3.1 The Spalart-Allmaras turbulence model

For steady flow, the continuity and Navier-Stokes equations are as follows:

$$\frac{\partial u_i}{\partial x_i} = 0 \quad (2)$$

$$\rho u_j \frac{\partial u_i}{\partial x_j} = \frac{\partial p}{\partial x_i} + \frac{\partial}{\partial x_j} \left( \mu \frac{\partial u_i}{\partial x_j} - \rho \overline{u'_i u'_j} \right) + S_u \quad (3)$$

Where  $\rho \overline{u'_i u'_j}$  is the Reynolds stress term. The SA model uses single dynamic equation to describe a kinematic-like variable called the SA variable,  $\tilde{\nu}$  to determine the turbulent viscosity  $\mu_t$  [11]:

$$\mu_t = \rho \tilde{\nu} f_{v1} \quad (4)$$

Where  $f_{v1}$  is the viscous damping function,

$$f_{v1} = \frac{\chi^3}{\chi^3 + C_{v1}^3} \quad (5)$$

$\chi$  is termed turbulent viscosity ratio, which is the ratio of  $\tilde{\nu}$  to the molecular kinematic viscosity of the working fluid,  $\nu$ :

$$\chi \equiv \frac{\tilde{\nu}}{\nu} \quad (6)$$

The steady flow transport equation for  $\tilde{\nu}$  is as follows:

$$\frac{\partial}{\partial x_i} (\rho \tilde{\nu} u_i) = G_\nu + \frac{1}{\sigma_{\tilde{\nu}}} \left[ \frac{\partial}{\partial x_j} \left\{ (\mu + \rho \tilde{\nu}) \frac{\partial \tilde{\nu}}{\partial x_j} \right\} + C_{b2} \rho \left( \frac{\partial \tilde{\nu}}{\partial x_j} \right)^2 \right] - Y_\nu + S_{\tilde{\nu}} \quad (7)$$

$G_\nu$  is the production of turbulent viscosity described by equation (8),  $Y_\nu$  is the destruction of turbulent viscosity in near-wall region due to wall blocking and viscous damping (see equation (13)), and  $S_{\tilde{\nu}}$  is a user-defined source term.

$$G_\nu = C_{b1} \rho \tilde{S} \tilde{\nu} \quad (8)$$

$\tilde{S}$  is defined as:

$$\tilde{S} \equiv S + \left( \frac{\tilde{\nu}}{\kappa^2 d^2} \right) \left( 1 - \frac{\chi}{1 + \chi f_{v1}} \right) \quad (9)$$

$S$  is a scalar measure of the deformation tensor based on the magnitude of the vorticity:

$$S = \sqrt{2\Omega_{ij}\Omega_{ij}} + 2 \min \left( 0, \sqrt{2S_{ij}S_{ij}} - \sqrt{2\Omega_{ij}\Omega_{ij}} \right) \quad (10)$$

$\Omega_{ij}$  is the mean rate-of-rotation tensor and  $S_{ij}$  is the mean strain rate:

$$\Omega_{ij} = \frac{1}{2} \left( \frac{\partial u_i}{\partial x_j} - \frac{\partial u_j}{\partial x_i} \right) \quad (11)$$

$$S_{ij} = \frac{1}{2} \left( \frac{\partial u_j}{\partial x_i} + \frac{\partial u_i}{\partial x_j} \right) \quad (12)$$

The  $Y_\nu$  term in equation (7) is modelled as follows:

$$Y_\nu = C_{w1} \rho f_w \left( \frac{\tilde{\nu}}{d} \right)^2 \quad (13)$$

Where,  $d$  is the distance to the closest surface

$$f_w = g \left( \frac{1 + C_{w3}^6}{g^6 + C_{w3}^6} \right)^{\frac{1}{6}} \quad (14)$$

$$g = r + C_{w2} (r^6 - r) \quad (15)$$

$$r \equiv \frac{\tilde{\nu}}{\tilde{S} \kappa^2 d^2} \quad (16)$$

$$C_{w1} = \frac{C_{b1}}{\kappa^2} + \frac{1 + C_{b2}}{\sigma} \quad (17)$$

The default values for the SA model constants  $C_{b1}$ ,  $C_{b2}$ ,  $\sigma_{\tilde{\nu}}$ ,  $C_{v1}$ ,  $C_{w2}$ ,  $C_{w3}$ , and  $\kappa$  are:  $C_{b1} = 0.1355$ ,  $C_{b2} = 0.622$ ,  $\sigma_{\tilde{\nu}} = 2/3$ ,  $C_{v1} = 7.1$ ,  $C_{w2} = 0.3$ ,  $C_{w3} = 2.0$ , and  $\kappa = 0.4187$ .

While the SA model is computationally efficient and robust for many practical engineering problems, its inherent assumption of isotropic turbulence, among other simplifications, limits its ability to predict complex, anisotropic, or transitional flow phenomena.

### 3.2 Atmospheric boundary layer model and turbulent length scale

Neutral atmospheric boundary layer (ABL) is assumed in this study [5], where the inlet boundary conditions are defined as follows:

$$u = \frac{u_*}{\kappa} \ln \left( \frac{y + z_0}{z_0} \right) \quad (18)$$

$$k = u_*^2 C_\mu^{-\frac{1}{2}} \quad (19)$$

$$\varepsilon = \frac{u_*^3}{\kappa(y + z_0)} \quad (20)$$

Where  $z_0$  denotes the aerodynamic roughness length. Given  $I_H$  and  $U_H$  denote the turbulent intensity and freestream velocity of the airflow at hub height,  $Y_H$ , the turbulent kinetic energy,  $k$ , dissipation rate,  $\varepsilon$ , and the turbulent viscosity,  $\mu_t$ , defined by using the standard  $k - \varepsilon$  (SKE) turbulence model are [12]:

$$k = \frac{3}{2} (U_H I_H)^2 \quad (21)$$

$$\varepsilon = C_\mu^{\frac{3}{4}} \frac{k^{\frac{3}{2}}}{\ell_T} \quad (22)$$

$$\mu_t = C_\mu \rho \frac{k^2}{\varepsilon} \quad (23)$$

Where  $\ell_T$  is the turbulent length scale. From the case where  $k$  and shear stress  $\tau$  are constant based on the assumption that  $\mu_t$  is proportional to height,  $y$  [13,14]:

$$\mu_t = \rho u_* \kappa y \quad (24)$$

The  $\ell_T$  at hub height  $Y_H$  in equation (22) can be obtained by substitute in equations (22) and (19) into equation (23) and equate it with equation (24):

$$\ell_T = \kappa Y_H \quad (25)$$

The friction velocity,  $u_*$  is calculated as follows:

$$u_* = \sqrt{\frac{3}{2} C_\mu^{\frac{1}{4}} I_H U_H} \quad (26)$$

## 4. Numerical simulation

### 4.1 Computational domain and mesh

The computational domain is presented in figure 1. Nibe B WT is used to conduct the mesh study, with  $D = 40\text{m}$ , and  $Y_H = 45\text{m}$ . The simulations are conducted with  $C_T = 0.82$  at  $U_H = 8.54\text{ m/s}$  and  $I_H = 11\%$ . The mesh study is conducted according to [15]. 3 different meshes with cell count inflation rate of  $\approx 2.7$  from coarse to fine meshes are used. CFD simulations are conducted using the 3 meshes, and the wake velocities,  $u$  at  $Y_H$  and downstream position of  $x=2.5D$  and  $7.5D$  are

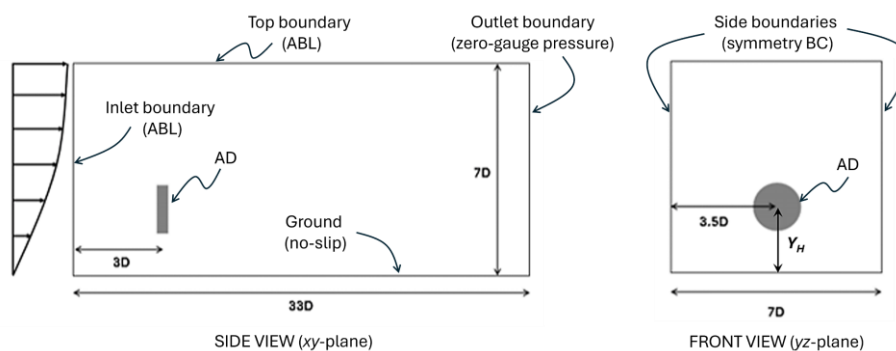


**Figure 1.** Computational domain and boundary conditions.

**Table 1.** Mesh convergence study with Richardson extrapolation.

Mesh resolution	Mesh index, $i$	Cell count, $N$	Normalised mesh, $N_1/N_i$	$f = u/U_H$		$\Delta f = (f_i - f_0)/f_0$ [ $\times 100\%$ ]	
				$x = 2.5D$	$x = 7.5D$	$x = 2.5D$	$x = 7.5D$
Coarse	3	375,186	7.58	4.2482	6.4600	2.3660	0.3233
Medium	2	1,066,893	2.67	4.1602	6.4409	0.2448	0.0256
Fine	1	2,845,026	1	4.1512	6.4394	0.0291	0.0025
Richardson	0	*	0	4.1500	6.4392	0	0

recorded. Then, Richardson extrapolation technique is used to estimate the final  $u$  for the idealised infinite mesh resolution (mesh 0):

$$f_0 \approx f_3 + \frac{f_3 - f_2}{r^P - 1} \quad (27)$$

Where  $r = (N_3/N_2)^{1/3}$  is the mesh refinement factor, and  $P$  is the order of convergence:

$$P = \frac{1}{\ln(r)} \ln \left( \frac{f_3 - f_2}{f_2 - f_1} \right) \quad (28)$$

The error between the 3 meshes and the extrapolated results are then computed to quantify the mesh accuracy, as shown in table 1. The average error  $\Delta f$  for mesh 2 is less than 0.5%. Therefore, its parameter settings are used to construct the meshes for the CFD simulations in this study. The element sizes for AD is 0.0125D; the ground face size is 0.5D, with 12 prism layers of 1.2 inflation rate to capture the near ground boundary layer. The 1<sup>st</sup> cell height of the prism layer is 0.004D, resulting in the  $y^+ \approx 100$ .

## 5. Results and discussion

Four existing wind turbines under varying operating conditions were used to validate the SA model by comparing the measurement data and results from the literature models.

### 5.1 Sexbierum WT

The field measurement data for Sexbierum WT ( $D=30$  m,  $Y_H = 35$  m,  $C_T = 0.75$ ,  $U_0 = 8.5$  m/s,  $I_H = 10\%$ ) from [16] are compared with computed data from SA model, the 2D\_k and 2D Jensen models [17] and a modified  $k - \omega$  model [18]. The 3 selected wake profiles are presented in figure 2. The results show that SA model closely matches with the 2D\_k Jensen profile at  $x = 5.5D$ , and closely resembles the modified  $k - \omega$  profiles at  $x=2.5D$  and  $8D$ . The average mean absolute percentage error (MAPE) obtained with SA, 2D\_k Jensen, 2D Jensen, and modified  $k - \omega$  models are 8.25%, 10.10%, 7.53%, and 7.05%, respectively. Overall, the wake profiles predicted by SA agree well with the experimental data.

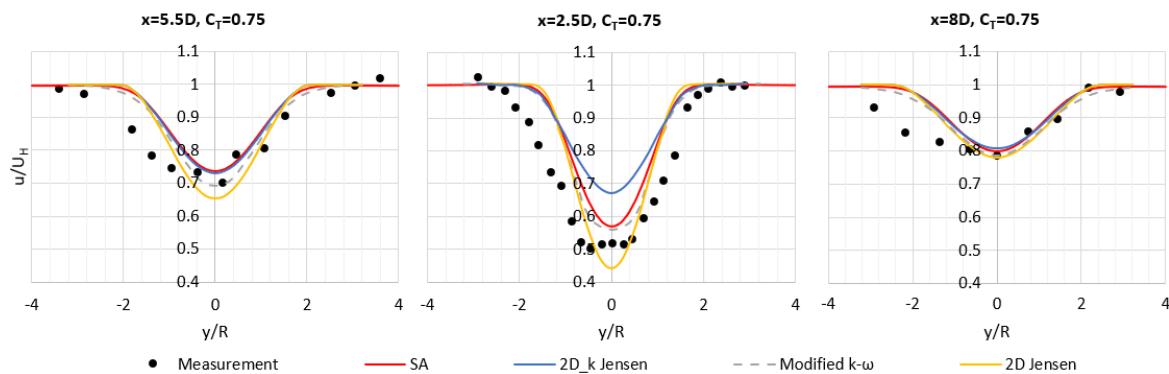


**Figure 2.** Comparison of Sexbierum WT wake profiles at various downstream locations.

### 5.2 Garrad-Hassan (GH) WT

Experimental data for Garrad-Hassan WT ( $D=43.2$  m,  $Y_H=50$  m,  $C_T = 0.62$  and  $0.85$ ,  $U_0 = 5.3$  m/s,  $z_0=0.075$  m) from [17] and [19] is compared with the computed data for SA model, and 2D\_k and 2D Jensen models [17]. Three selected wake profiles are presented in figure 3. The results show that the 2D\_k Jensen model greatly under predicts the wake profiles at  $x = 5D$  and  $7.5D$  for  $C_T = 0.62$ , while the 2D Jensen model greatly overpredicts the wake profile at  $x = 7.5D$  for  $C_T = 0.85$ . The average MAPEs for the SA, 2D\_k Jensen, and 2D Jensen models for  $C_T = 0.62$  at  $x = 5D$ ,  $7.5D$ ,  $10D$ , and  $C_T = 0.85$  at  $x = 5D$  and  $7.5D$  are 2.10%, 2.63%, and 4.24%, respectively. In general, SA aligns well with the experimental data.

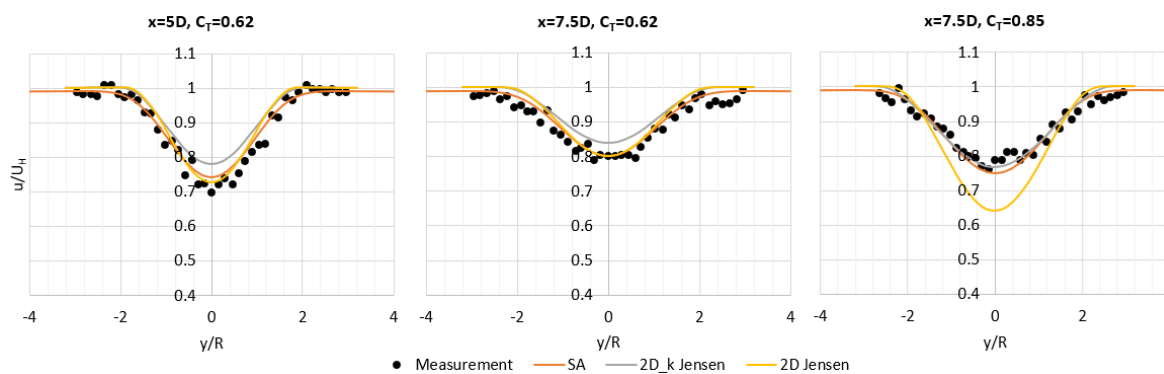


**Figure 3.** Comparison of GH wind turbine wake profiles at various downstream locations.

### 5.3 Nibe B WT

Field measurements for the Nibe B WT from [20] (extracted from [5]) re compared with computed data from the SA model, SKE and Ren models [5], Kasmi model [7], and the Large Eddy Simulation (LES) [10]. The WT ( $D = 43.2$  m and  $Y_H = 50$  m) operates at  $C_T = 0.77$  ( $U_0 = 11.52$  m/s) and  $C_T = 0.82$  ( $U_0 = 8.54$  m/s) with  $I_H = 11\%$ . Three selected wake profiles are presented in figure 4. The results show that SKE greatly underpredicts the wake at  $x = 7.5D$  for  $C_T = 0.77$ ; for  $C_T = 0.82$ , LES slightly underpredicts the wake at  $x = 2.5D$ , while the Kasmi model overpredicts the wake at  $x = 6D$ . The average MAPEs for SA, Ren, Kasmi, SKE and LES models for  $C_T = 0.77$  and  $0.82$  at

$x = 2.5D, 6D, 7.5D$ , are 5.49%, 5.74%, 6.07%, 9.59%, and 3.72%, respectively. In general, the proposed method agrees well with the experimental data.

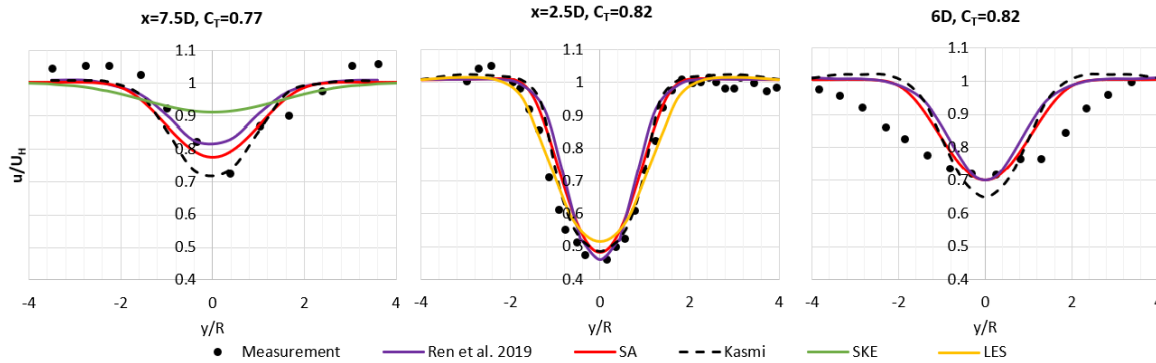


**Figure 4.** Comparison of Nibe B WT wake profiles at various downstream locations.

#### 5.4 Danwin 180kW WT

Field measurements for the Danwin WT ( $D = 31$  m,  $Y_H = 23$  m) from [6], are compared with computed data from Ren model [5], the extended  $k - \varepsilon$  model (Kasmi model) [7], and full-rotor CFD [21], operating at  $C_T = 0.82$  ( $U_0 = 8$  m/s,  $I_H = 7\%$ ), and  $C_T = 0.65$  ( $U_0 = 11$  m/s,  $I_H = 6\%$ ). Three selected wake profiles are presented in figure 5. The results show that the wake profiles predicted by SA match the experimental data. The average MAPE obtained with SA model, Ren model, Kasmi model, full-rotor CFD for  $C_T = 0.65$  at  $x = 6.2D$  and  $C_T = 0.65$  at  $x = 1D, 4.15D$ , and  $9.4D$ , are 6.38%, 6.34%, 7.27%, and 6.55%, respectively.

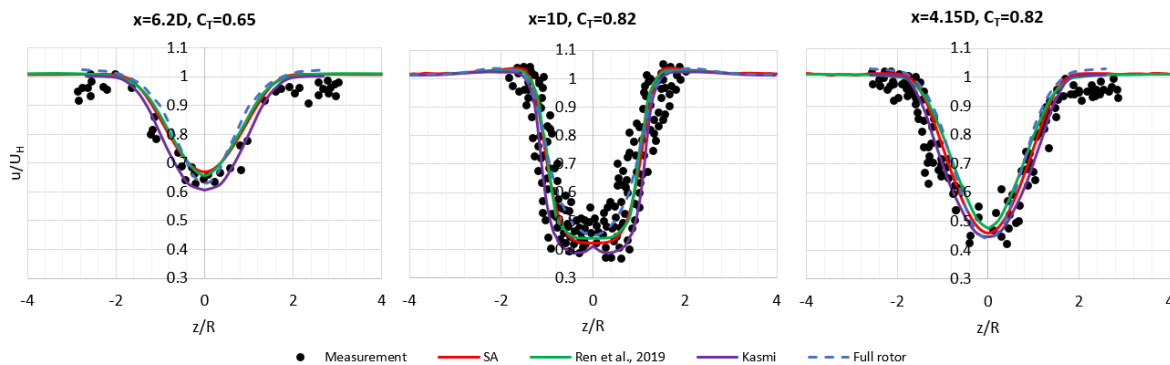


**Figure 5.** Comparison of Danwin 180kW wind turbine wake profiles at various downstream locations.

## 6. Conclusions

The SA turbulence model has been successfully applied to horizontal axis WT wake modelling using the AD approach. The accuracy of the proposed model was validated using data from four WTs of various sizes and operational conditions.

The overall average MAPE for SA is 5.55%, compared to 2D\_k Jensen (6.37%), 2D Jensen (5.88%), modified  $k-\omega$  (7.04%), Ren et al. (6.21%), El Kasmi and Masson (6.5%), full-rotor

(6.56%), default SKE (9.59%), and LES (3.72%). This confirms the SA model can capture wake profiles effectively.

The required  $\ell_T$  for the proposed SA model was derived from the  $k$  and  $\varepsilon$  based on the neutral ABL assumption and SKE turbulence model. Further investigations are needed to extend the model for non-neutral ABL conditions, as well as validating its accuracy in wind farms where the flow is complex and wake interference is prominent.

## 7. References

- [1] Yan C and Archer C L 2018 Assessing compressibility effects on the performance of large horizontal-axis wind turbines *Appl. Energy* **212** 33–45
- [2] Shapiro C R, Starke G M, Meneveau C and Gayme D F 2019 A Wake Modeling Paradigm for Wind Farm Design and Control *Energies* **12** 2956
- [3] Moens M, Duponcheel M, Winckelmans G and Chatelain P 2018 An actuator disk method with tip-loss correction based on local effective upstream velocities *Wind Energy* **21** 766–82
- [4] Tzimas M and Prospathopoulos J 2016 Wind turbine rotor simulation using the actuator disk and actuator line methods *J. Phys. Conf. Ser.* **753** 032056
- [5] Ren H, Zhang X, Kang S and Liang S 2018 Actuator Disc Approach of Wind Turbine Wake Simulation Considering Balance of Turbulence Kinetic Energy *Energies* **12** 16
- [6] Magnusson M, Rados K G and Voutsinas S G 1996 A Study of the Flow Downstream of a Wind Turbine Using Measurements and Simulations *Wind Eng.* **20** 389–403
- [7] El Kasmi A and Masson C 2008 An extended model for turbulent flow through horizontal-axis wind turbines *J. Wind Eng. Ind. Aerodyn.* **96** 103–22
- [8] Shapiro C R, Gayme D F and Meneveau C 2019 Filtered actuator disks: Theory and application to wind turbine models in large eddy simulation *Wind Energy* **22** 1414–20
- [9] Stevens R J A M, Martínez-Tossas L A and Meneveau C 2018 Comparison of wind farm large eddy simulations using actuator disk and actuator line models with wind tunnel experiments *Renew. Energy* **116** 470–8
- [10] Troldborg N, Sørensen J N, Mikkelsen R and Sørensen N N 2014 A simple atmospheric boundary layer model applied to large eddy simulations of wind turbine wakes *Wind Energy* **17** 657–69
- [11] Spalart P and Allmaras S 1992 A one-equation turbulence model for aerodynamic flows *30th Aerospace Sciences Meeting and Exhibit* 30th Aerospace Sciences Meeting and Exhibit (Reno, NV, U.S.A.: American Institute of Aeronautics and Astronautics)
- [12] Katul G G, Mahrt L, Poggi D and Sanz C 2004 ONE- and TWO-Equation Models for Canopy Turbulence *Bound.-Layer Meteorol.* **113** 81–109
- [13] Kaimal J C and Finnigan J J 1994 *Atmospheric Boundary Layer Flows: Their Structure and Measurement* (Oxford University Press)
- [14] Zhang X 2009 *CFD simulation of neutral ABL flows* (Risø DTU)
- [15] Roache P J 2009 *Fundamentals of Verification and Validation* (Socorro, New Mexico, USA: Hermosa)
- [16] Cleijne J W 1993 *Results of Sexbierum Wind Farm; single wake measurements* (TNO Institute of Environmental and Energy Technology)
- [17] Tian L, Zhu W, Shen W, Zhao N and Shen Z 2015 Development and validation of a new two-dimensional wake model for wind turbine wakes *J. Wind Eng. Ind. Aerodyn.* **137** 90–9
- [18] Prospathopoulos J M, Politis E S, Rados K G and Chaviaropoulos P K 2011 Evaluation of the effects of turbulence model enhancements on wind turbine wake predictions *Wind Energy* **14** 285–300
- [19] Schlez W, Tindal A and Quarton D 2003 *GH Wind Farmer Validation Report* (Bristol, UK: Garrad Hassan and Partners Ltd)
- [20] Taylor G J 1990 *Wake measurements on the Nibe wind turbines in Denmark* (UK: National Power - Technology and Environment Centre)
- [21] AbdelSalam A M and Ramalingam V 2014 Wake prediction of horizontal-axis wind turbine using full-rotor modeling *J. Wind Eng. Ind. Aerodyn.* **124** 7–19

## Acknowledgement

The project is funded by the Ministry of Higher Education Malaysia, under the Fundamental Research Grant Scheme (FRGS Grant No. FRGS/1/2023/TK08/SEGI/02/1).